

On the computation of buoyancy-driven turbulent flows in rectangular enclosures

N. Z. Ince and B. E. Launder

Department of Mechanical Engineering, UMIST, Manchester, UK

Numerical computations are reported of turbulent natural convection of air in two tall rectangular enclosures with heated and cooled vertical walls. The very different aspect ratios considered, 30:1 and 5:1, lead to appreciable differences in flow structure in the two cases. It is found that a version of the Jones-Launder low-Reynolds-number $k-\epsilon$ model, used previously to compute heat transfer rates downstream of an abrupt expansion, leads to a very satisfactory agreement with reported experimental data of the velocity and thermal field, including the distribution of the Nusselt number.

Keywords: natural convection; turbulent flow; cavity flow; numerical modeling

Introduction

Turbulent, confined, buoyancy-driven, or buoyancy-modified, flows arise in many engineering structures ranging in scale from 1-mm diameter coolant passages in turbine blades to large auditoria. Buoyant forces affect both the general movement of the fluid within the enclosure and the turbulent mixing processes. It is thus by no means certain that a turbulence model developed for flows with negligible stratification will extrapolate correctly to situations where buoyant effects are strong.

In cases where the buoyant motion arises from heat transfer through vertical or nearly vertical walls, the greatest effects of buoyancy occur very close to the wall where viscous effects are appreciable. This renders inapplicable the use of local-equilibrium logarithmic velocity and temperature-versus-distance variations extensively used to simplify the calculation of near-wall flows. While George and Capp¹ have proposed an alternative inner-layer scaling for naturally driven flow, the more convincing modeling attempts have instead extended numerical computations up to the wall itself, applying molecular transport boundary conditions there. Here we mention the studies of To and Humphrey² of the natural boundary layer on a vertical plate, Cotton and Jackson^{3,4} of turbulent mixed convection in vertically upward flow through heated tubes, and our colleagues Betts, Dafa'Alla, and Haroutunian,^{5,6} who have considered fully developed natural convection between infinite vertical parallel planes with one heated and one cooled wall. As in the earlier work of Plumb and Kennedy,⁷ all of these studies solved low-Reynolds-number forms of the turbulence-energy (k) and energy-dissipation-rate (ϵ) equations and, while the main thrust of the To-Humphrey study was on results obtained employing an algebraic second-moment (ASM) closure, that investigation, like the others cited, presented results for the simpler and more widely applied eddy-diffusivity model.

For the test cases examined by To and Humphrey and Cotton and Jackson, very satisfactory agreement with experiment resulted from the use of the $k-\epsilon$ eddy-viscosity model (EVM). The same could not be said for the fully developed buoyant cavity study of Betts and Dafa'Alla, however, for peak velocities were appreciably too low and heat fluxes too high. Indeed, this work brought out what a sensitive test case this was for

discriminating between alternative versions of the $k-\epsilon$ eddy-viscosity model, the overprediction of the wall heat flux ranging from 40 to 100% for the versions tested.* An important difference between the buoyant cavity flow and the other two studies noted above is that, in the former, the maximum turbulent energy is to be found at the center plane; we shall argue that this feature is a substantial contributor to the poor agreement reported in Ref. 6.

The flow geometry considered in the present study is the buoyantly driven rectangular cavity. We cover both the narrow cavity case examined experimentally by Ince⁹ and Betts and Dafa'Alla^{6,10} (which approximates in its midregion the flow in an infinitely tall rectangular enclosure) as well as a cavity of 5:1 aspect ratio for which LDA data have been reported by Cheesewright *et al.*¹¹ As in the simpler flows discussed above, a low-Reynolds-number model is required. We decided to retain a $k-\epsilon$ EVM (though with a simply buoyant flow adaptation) initially with a view to using these results as a yardstick against which the performance of a second-moment closure could be judged. As it turned out, agreement with the data fell within the uncertainties in the experimental values associated with possible small departures from two-dimensionality and from the precise boundary conditions. Further refinement to the modeling within the context of the presently considered test cases was thus not possible.

The second section describes briefly the turbulence model adopted, while the main features of the numerical solver and the grid independence tests performed are presented in the third section. The principal computational results are reported and compared with experiments in the fourth section, together with a reconsideration of the George and Capp wall laws.

Turbulence model

In Cartesian tensor notation the equations describing the mean flow and temperature within the cavity are

$$\frac{\partial}{\partial x_j} (\rho U_j U_i) = -\frac{\partial P}{\partial x_i} + \rho g_i + \frac{\partial}{\partial x_j} \left(\mu \left[\frac{\partial U_i}{\partial x_j} + \frac{\partial U_j}{\partial x_i} \right] - \rho \overline{u_i u_j} \right) \quad (1)$$

$$\frac{\partial}{\partial x_j} (\rho c_p U_j \Theta) = \frac{\partial}{\partial x_j} \left(\kappa \frac{\partial \theta}{\partial x_j} - \rho c_p \overline{u_j \theta} \right) \quad (2)$$

Address reprint requests to Dr. Ince at the Department of Mechanical Engineering, UMIST, Manchester M60 1QD, UK.

Received 16 December 1987; accepted for publication 27 July 1988

© 1989 Butterworth Publishers

* These were the same model proposals previously examined by Patel *et al.*⁸ for boundary layers in pressure gradients.

We note that in the two-dimensional computations the Boussinesq approximation is not made in any of the transport equations, though density fluctuations are accounted for only in the gravitational term (see Equation 7).

With two exceptions the Reynolds stresses and heat fluxes are obtained from the Jones-Launder¹² low-Reynolds-number *k-ε* model with the modified coefficients recommended in Ref. 13. The turbulent stresses and heat fluxes are given by

$$\overline{\rho u_i u_j} = \frac{2}{3} \delta_{ij} \rho k - \mu_t \left(\frac{\partial U_i}{\partial x_j} + \frac{\partial U_j}{\partial x_i} \right) \quad (3)$$

$$\overline{\rho u_j \theta} = - \frac{\mu_t}{\sigma_\theta} \frac{\partial \theta}{\partial x_j} \quad (4)$$

where $\mu_t = c_\mu \rho k^2 / \bar{\epsilon}$ and σ_θ , the turbulent Prandtl number, is taken as a constant.

In Ref. 11 the turbulence energy *k* and $\bar{\epsilon}$ (the part of the (kinematic) energy dissipation rate associated with spectral transfer) are obtained from their own transport equations as follows:

$$\frac{\partial}{\partial x_j} (\rho U_j k) = \frac{\partial}{\partial x_j} \left(\left(\mu + \frac{\mu_t}{\sigma_k} \right) \frac{\partial k}{\partial x_j} \right) + P_k - \rho \epsilon \quad (5)$$

$$\begin{aligned} \frac{\partial}{\partial x_j} (\rho U_j \bar{\epsilon}) = & \frac{\partial}{\partial x_j} \left(\left(\mu + \frac{\mu_t}{\sigma_\epsilon} \right) \frac{\partial \bar{\epsilon}}{\partial x_j} \right) + c_{\epsilon 1} \frac{\bar{\epsilon}}{k} P_k - c_{\epsilon 2} \rho \frac{\bar{\epsilon}^2}{k} \\ & + \frac{2\mu\mu_t}{\rho} \left(\frac{\partial^2 U_i}{\partial x_k^2} \right)^2 \end{aligned} \quad (6)$$

In these equations, ϵ , the total dissipation rate of *k*, equals $\bar{\epsilon} + 2\nu(\partial k^{1/2}/\partial x_k)^2$ while P_k denotes the generation rate of turbulence energy, in the present case due to buoyancy as well as shear effects:

$$P_k \equiv -\rho \overline{u_i u_j} \frac{\partial U_j}{\partial x_i} - \alpha \frac{\rho}{\Theta} \overline{u_i \theta} g_i \quad (7)$$

where α is the dimensionless volumetric expansion coefficient of the fluid medium with respect to temperature. Air is the fluid medium for the two cases here considered, and the value of α is taken as unity; i.e., the air is regarded as an ideal gas. The following standard values proposed in Ref. 13 are adopted for

the empirical coefficients:

$$c_\mu = 0.09 \exp\left(-\frac{3.4}{(1 + R_t/50)^2}\right), \quad c_{\epsilon 1} = 1.44$$

$$c_{\epsilon 2} = 1.92[1 - 0.3 \exp(-R_t^2)], \quad R_t = \rho k^2 / \mu \bar{\epsilon}$$

$$\sigma_k = 1.0, \quad \sigma_\epsilon = 1.3, \quad \sigma_\theta = 0.9$$

Rodi and Scheuerer's⁸ survey of alternative *k-ε* models concluded that these values gave as successful a prediction of various boundary layers as any of the 10 variants they tested.

We note at this point the two nonstandard features of the model. First, the introduction of Equation 4 into Equation 7 would give an expression for the buoyant generation that vanished if the vertical temperature gradient was zero. It is well known, however, that in a simple shear flow with only cross-stream temperature variations the heat flux in the flow direction is usually significantly larger than in the cross-stream direction. The neglect of this streamwise flux (which results from using an eddy-diffusivity model) is of no consequence in predicting the mean flow in the absence of buoyant effects because the *gradient* of the flux (which is what appears in the mean enthalpy equation) is negligible compared with cross-stream gradients. In Equation 7, however, it is the flux itself rather than its gradient that appears. In naturally driven conditions the term may be of significance and, in vertical shear layers, modeling its effect via an EVM will be inadequate. Lin and Churchill¹⁴ assumed the vertical flux of heat to equal that of the horizontal flux, but this representation neglects the fact that in a vertical shear flow (as in the present case) the streamwise flux will *generally change sign* if the velocity gradient does, whereas the cross-stream flux will be virtually unaffected. We adopt instead the generalized gradient diffusion hypothesis (GGDH), apparently first introduced by Daly and Harlow.¹⁵

$$\overline{u_i \theta} = -c_\theta \frac{k}{\epsilon} \frac{\partial \theta}{\partial x_k} \quad (8)$$

which, unlike Equation 4, *does* give a vertical flux driven by a horizontal temperature gradient in the presence of shear. Here $\overline{u_i u_k}$ is given by Equation 3. In order to depart as little as possible from the eddy-viscosity formulation, the coefficient c_θ has been set equal to $\frac{3}{2}(c_\mu/\sigma_\theta)$ so that, in a *horizontal* shear flow, where the principal temperature and velocity gradients are

Notation

c_p	Specific heat at constant pressure
D	Width of enclosure
g	Gravitational acceleration
g_i	Gravitational acceleration vector (0, -g, 0)
H	Height of enclosure
k	Turbulent kinetic energy
P	Mean pressure
P_k	Generation rate of turbulent kinetic energy
Pr	Molecular Prandtl number
R_t	Turbulent Reynolds number, $\rho k^2 / \mu \bar{\epsilon}$
Ra_y	Local Rayleigh number, $2g\alpha \Delta\theta_w y^3 / \theta v^2$
Ra	$2g\alpha \Delta\theta D^3 / \theta v^2$
Ra_q	Heat-flux-based Rayleigh number $\overline{Ra} \overline{Nu}$
U_i	Mean velocity in direction x_i
$\overline{u_i j}$	Kinematic Reynolds stress
$\overline{j_j \theta}$	Kinematic turbulent heat flux
V	Vertical mean velocity
V^*	Vertical velocity in George and Capp coordinates; see Equation 13

x	Horizontal coordinate with origin at left (hot) surface
x_i	Cartesian space coordinate
y	Vertical coordinate with origin at lower edge of cavity
α	Dimensionless volumetric expansion coefficient, = 1 for ideal gas
$\Delta\Theta$	Temperature excess above ambient or midplane value
ϵ	Turbulence energy dissipation rate
$\bar{\epsilon}$	Part of ϵ associated with spectral transfer $\bar{\epsilon} \equiv \epsilon - 2\nu(\partial k^{1/2}/\partial x_j)^2$
θ	Temperature fluctuation
Θ	Local mean temperature (absolute scale)
κ	Thermal conductivity
λ	Thermal diffusivity $\kappa/\rho c_p$
μ	Dynamic viscosity
μ_t	Turbulent viscosity
ν	Kinematic viscosity
ρ	Density
σ_ϕ	Turbulent Prandtl number for ϕ transport ($\phi = \theta, k, \epsilon$)

vertical, Equation 8 should give the same result in the buoyant source term as Equation 4.

The second and more important modification made to the standard $k-\epsilon$ model is the inclusion of a near-wall source term in the ϵ equation. It is known that in boundary layers approaching separation the $k-\epsilon$ model returns near-wall length scales that are too large.^{16,17} In separated flows the problem is more serious, particularly if an equation for ϵ is solved up to the wall in place of wall functions. Yap,¹⁸ studying heat transfer rates downstream from an abrupt pipe enlargement, obtained predicted Nusselt numbers some five times higher than experiment in the vicinity of the reattachment point. He therefore added a source S_ϵ to the right side of the transport equation for $\tilde{\epsilon}$, Equation 6:

$$S_\epsilon = 0.83 \left(\frac{k^{3/2}}{\epsilon c_1 y} - 1 \right) \left(\frac{k^{3/2}}{\epsilon c_1 y} \right)^2 \frac{\tilde{\epsilon}^2}{k} \quad (9)$$

where y is the distance from the wall and c_1 ($=2.5$) is the slope of the turbulent length scale $k^{3/2}/\epsilon$ in the near-wall region of a constant-stress shear flow (it is analogous to the von Karman constant in the mixing length hypothesis). Thus, the term is zero in a wall flow in local equilibrium and is uninfluential in the outer region because there $k^{3/2}/\epsilon$ increases less rapidly than y , and so the final product in Equation 9 diminishes rapidly. In a near-wall separated region where $k^{3/2}/\epsilon$ given by Equation 6 might typically be four times larger than $c_1 y$, S_ϵ acts to increase ϵ , thereby decreasing k (and $k^{3/2}/\epsilon$); it thus drives the length scale level toward its local equilibrium value. Although the term is purely phenomenological, it has been found beneficial in predicting other shear flows affected by force fields currently under study in Manchester.¹⁹

Now, the flow considered here is not a separated flow, and it may not be evident that the additional source term should be influential. The reason that it is, is that the largest levels of turbulence energy in the infinite buoyant cavity occur in the central region. As in a separated flow, therefore, there is a strong diffusion of turbulence energy toward the wall, and it seems to be in these circumstances that Equation 6 returns levels of $\tilde{\epsilon}$ that are too low. To be consistent with the intention of Equation 9, we have included sources associated with both of the vertical walls, but, where it matters (i.e. close to one of the walls), it is only the contribution from the nearest wall that is significant.

The numerical procedure

Numerical solutions to the cavity flows reported below were obtained using the extensively applied TEAM code of Huang and Leschziner,²⁰ a two-dimensional finite-volume elliptic solver employing primitive variables (velocity components and pressure) distributed on the usual staggered grid. The solution proceeds iteratively by updating variables a line at a time, the variables being solved sequentially.

The wall-function sequences in the original program were replaced by the appropriate boundary conditions at the wall ($U_i = k = \tilde{\epsilon} = 0$; Θ as noted below) while the low-Reynolds-number terms were coded into the k and $\tilde{\epsilon}$ source arrays.

All two-dimensional computations reported here were performed on a carefully graded 60×60 mesh (Figure 1), this being the finest achievable with the computer resources available to us. For the infinite buoyant cavity only one plane of nodes was required, and, for this case, successive runs were made with the equivalent of* 60, 100, 150, and 180 nodes between the vertical

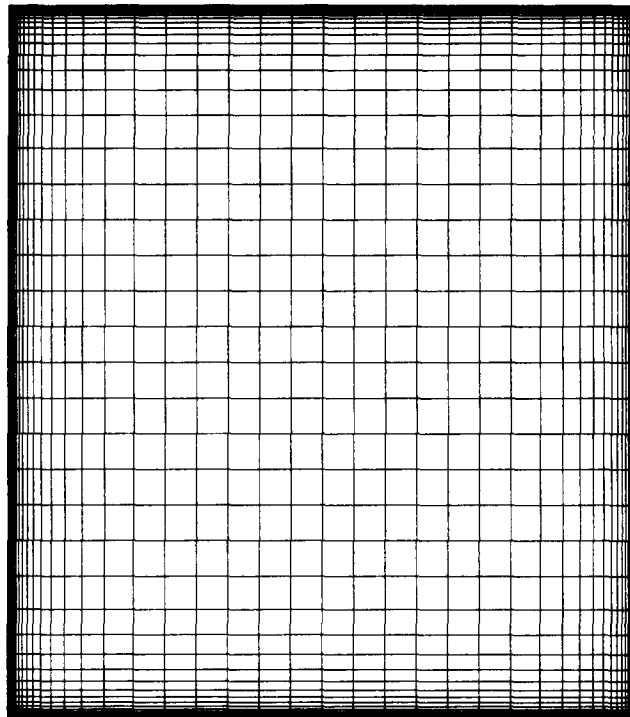


Figure 1 Mesh distribution

walls. In fact, refinement from 60 to 100 nodes produced changes in maximum velocity and Nusselt number of only about 1%; further refinements brought negligible further change. The gratifyingly small grid resolution error with 60 nodes is probably associated with the relatively modest levels of Rayleigh number considered here; as a result, the effective viscosity changes over the flow by only one order of magnitude and the sublayers, where molecular transport is the dominant mechanism, occupy a larger proportion of the flow than in forced-convection boundary layers.

Presentation and discussion of results

The first task was to check the one-dimensional finite-element predictions of Betts and Dafa'Alla⁶ for the infinite buoyant cavity. The same rate of heat flow into and out of the cavity was prescribed at the cavity walls. The results, given in Table 1, confirmed the conclusion of Ref. 6 that the Launder-Sharma¹³ version of the $k-\epsilon$ EVM (while performing the best of the forms tested in Ref. 6) seriously overpredicted heat transfer rates and underpredicted the maximum velocity. This anomalous behavior arises, one must suppose, from generally overpredicted levels of turbulent viscosity.

The next step was to include the two amendments of the turbulence model discussed earlier: the Yap¹⁸ ϵ source (Equation 9) and the GGDH representation of $\bar{u}_i \theta$ (Equation 8), in the buoyant source. From Table 1 we see that inclusion of the former brings a striking improvement in agreement; indeed, the computations now show a marginally higher velocity and lower heat flux than the measurements.⁹ Some of this small discrepancy is removed by introducing the modified buoyant source into Equation 7. The Cartesian coordinate expression for the buoyant source of k is in this case

$$\frac{c_\theta c_\mu}{\Theta} g \frac{k^3}{\epsilon^2} \frac{\partial V}{\partial x} \frac{\partial \Theta}{\partial x}$$

* In fact, for the one-dimensional computations the Boussinesq approximation was made and viscosity taken as constant leading to anti-symmetric flow about the midplane of the channel. Consequently, our grid extended only from one wall to the midplane.

Table 1 Nusselt number and maximum velocity in infinite buoyant cavity

Basis	Nu	V_{max} (cm/s)
Experiment in 30:1 cavity (midheight value)	4.9	11.40
Computation: standard $k-\epsilon^{13}$	6.53	8.96
Computation: inclusion of ϵ source (Equation 9)	4.66	12.40
Computation: inclusion of Equation 9 and use of Equation 8 in P_k	4.74	12.10

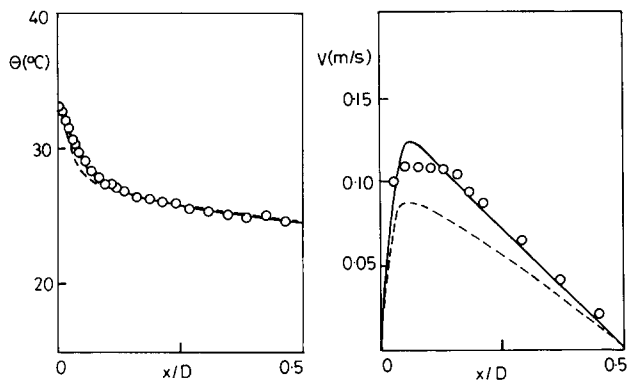


Figure 2 Measured and computed profiles in an infinite cavity: (a) temperature; (b) vertical velocity; symbols experiments^{9,9}; --- $k-\epsilon$ EVM without Yap correction; — $k-\epsilon$ EVM including Yap correction

Since $\partial\Theta/\partial x$ is negative everywhere and $\partial V/\partial x$ is also negative over most of the region where turbulent transport is significant, the term raises the turbulence energy slightly leading to the indicated changes in maximum mean velocity and Nusselt number. The corresponding mean velocity and temperature distributions are shown in Figure 2. The experimental results are those obtained by averaging the profiles for the upflowing and downflowing halves of the cavity. As we shall see, these are not quite the same.

Attention was turned next to computing the flow in the complete 30:1 two-dimensional cavity for which data are reported in Refs. 9 and 10. The thermal boundary condition prescribed on the heated side was that of uniform heat flux, while on the cooled side of the enclosure the measured (nearly uniform) wall temperature was applied. The short, well-insulated end walls were assumed adiabatic.* In these computations the variation of mean density and viscosity over the flow was included. Figures 3 and 4 show the mean velocity and temperature profiles at midheight and at two planes near the top and bottom of the cavity. The data at the midplane are those shown in averaged form in Figure 2: the differences in the profile in the vicinity of the velocity maximum on the hot and cold side are now clearly visible. While the computations do not exhibit

* In fact, although the original data were taken in a 30:1 cavity,⁹ the later addition of further insulation to the top and bottom end walls reduced the aspect ratio to 28.9:1. This small change in geometry, which only became known to the authors after all the computations had been made, is not expected to have had any significant effect.

precise antisymmetry (the variation in mean density ensures that), the distribution on the two sides is a good deal more similar than the data. The latter are evidently not compatible with a two-dimensional mass conservation, since at midheight on the hot side the measured velocity is never less than the computed value, while on the cold side it is never greater. The broken line shows the predicted behavior if the Yap correction, Equation 9, is not included: the benefits from the inclusion are evident.

The problem with lack of two-dimensionality of the data is also evident at the planes near the top and bottom of the cavity. There are, however, interesting features shown by the computed and measured velocity fields which are not clouded by the mass imbalance of the experiments. If the boundary conditions on each side of the cavity had been the same (e.g., both walls uniform heat flux or both uniform temperature) and the variation of density was negligible, the velocity profile along $y/D=0.05$ would be the mirror image of that along 0.95. In fact, although the shapes at the two stations are rather similar, the levels of velocity are roughly 30% greater near the top than near the bottom. The experiments and computations are in accord in this respect. The thin upward-moving shear layer adjacent to the hot wall near the bottom of the cavity and the downward-moving flow near the top of the cold wall are, according to the predictions (Figure 5), essentially laminar. The close agreement with experiment suggests that this accords with the actual situation.

The level of agreement between the measured and computed temperature profiles shown in Figure 4 is probably satisfactory in view of the lack of perfect two-dimensionality of the velocity field noted above. The differences in the profile shapes at 0.05

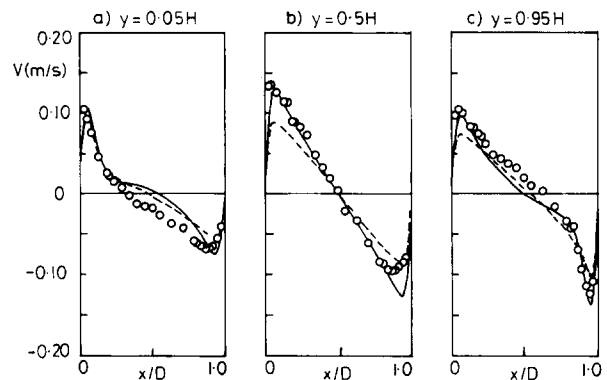


Figure 3 Measured and computed velocity profiles at three heights in 30:1 cavity. Key as Figure 2

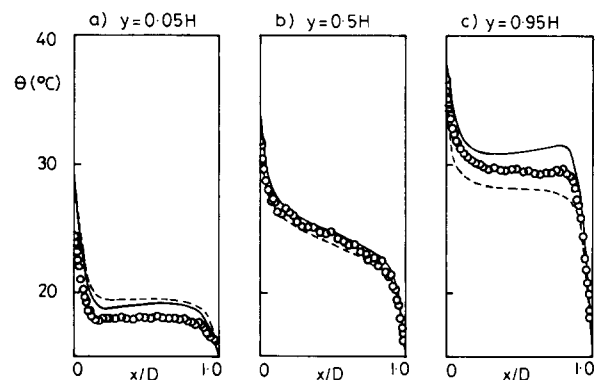


Figure 4 Measured and computed temperature profiles at three heights in 30:1 cavity. Key as Figure 2

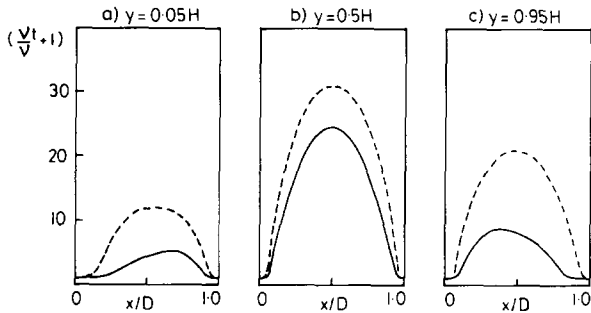


Figure 5 Computed profiles of effective viscosity $(\nu_e + \nu)/\nu$. Key as Figure 2

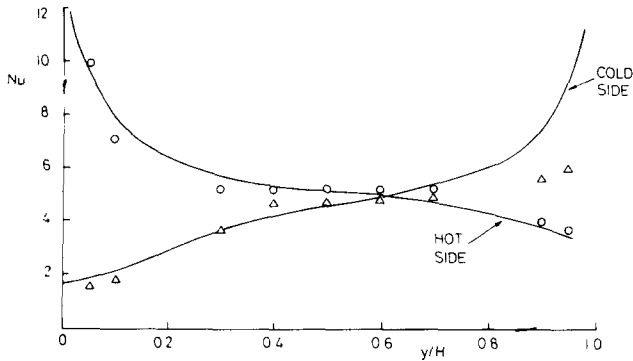


Figure 6 Nusselt number in 30:1 cavity: — computations; Δ cold wall; \circ hot wall; where Δ and \circ are experiments in Ince⁹

and 0.95 reflect the differences of the thermal boundary conditions at the heat-conducting walls. Figure 5 compares the profiles of effective viscosity across the same three planes as before with and without the Yap correction: a greater percentage reduction in viscosity from including the ϵ source occurs near the ends of the cavity than at the center. The figure confirms the laminar character of the rising shear layer at 0.05 and the falling one at 0.95.

Turning now to the heat transfer coefficients, Figure 6 presents the variation of Nusselt number along the heated and cooled vertical walls. Here the temperature difference in Nu is that between the wall in question and the centerline. There is a close correspondence between the computed and measured variations except near the top of the enclosure on the cooled wall. The cause of this discrepancy seems to be that a small heat leakage through the top wall of the enclosure (ignored in the computation) reduces the normal temperature gradient at the top of the cool wall, thus lowering the heat transfer rate.

Cheesewright *et al.*¹¹ have made extensive complementary studies in a cavity with a 5:1 aspect ratio. In their experiments the boundary layers on the two vertical walls do not directly interact, and, in contrast to the 30:1 cavity considered above, the central region is one of nearly uniform temperature and relatively low turbulence levels. The experiments were performed with carefully controlled uniform temperatures on the two primary vertical walls. Despite 200 mm of expanded Polystyrene on the top of the cavity, however, the authors report there was evidence of a small unquantified heat loss through this surface, which, while negligible by comparison with the total heat flow through the cavity, nevertheless significantly reduced the stable stratification of the fluid flowing slowly along the top wall. Consequently, the collapse of turbulence was by no means as complete as at corresponding positions at the bottom of the

cavity. In the absence of more precise information, the computations were made with adiabatic top and bottom walls. Comparisons with data are thus confined to the midplane where end effects should be negligible. Figure 7 compares the predicted velocity distribution with the measurements reported by Cheesewright *et al.*¹¹ after these authors had applied a correction for three-dimensional effects. The agreement is extremely close, including the weak under/overshoot in velocity in the core region. The corresponding temperature profiles in Figure 8 indicate that the core is at virtually a uniform temperature, though with slight undulations associated with the weak secondary vortices. The core level temperature is, however, significantly less than our predictions. While such unequal temperature drops across the near-wall sublayers could arise if the boundary layer on one side were distinctly more turbulent than the other, this seems unlikely to be the main cause of the discrepancy. If it were, the velocity at the midplane would also be affected and, as we have seen, the predicted velocity field is in excellent accord with the measurements. The most likely source of the discrepancy seems to be heat loss in the experiments through the side walls, which, according to the experimenters,^{11,21} amounted to more than 15% of the total heat input to the fluid. Such loss would obviously lower the mean level of temperature in the cavity.

The computed streamline pattern over the cavity is shown in Figure 9, where, for clarity, the length of the arrows has been plotted proportional to the square root of the velocity rather than to the velocity itself. The complex pattern of weak secondary motions is in marked contrast to the single cell produced in the 30:1 cavity.

Because the thermal layers on the two vertical walls do not

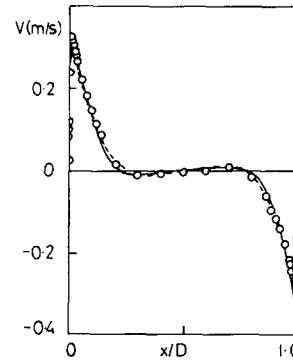


Figure 7 Midheight mean velocity profile in 5:1 cavity: \circ experiment Cheesewright *et al.*¹¹; --- $k-\epsilon$ EVM without Yap correction; — $k-\epsilon$ EVM including Yap correction

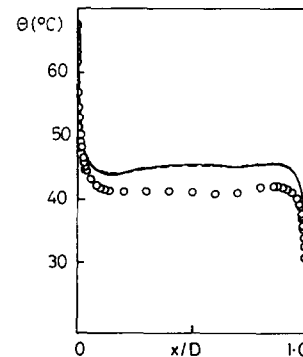


Figure 8 Midheight mean temperature profile in 5:1 cavity. Key as Figure 7

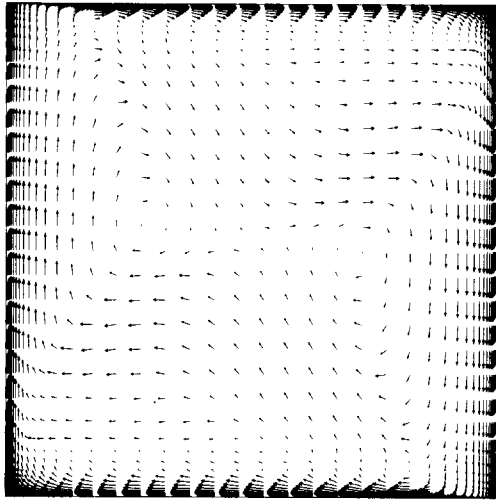


Figure 9 Computed streamline pattern in 5:1 cavity. N.B. Arrow length $\propto \sqrt{\text{velocity}}$

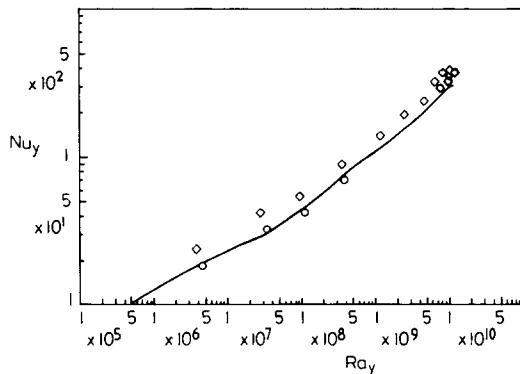


Figure 10 Local Nusselt number in 5:1 cavity: — computation; \diamond hot and \circ cold from experiments²¹

interact, Cheesewright *et al.*¹¹ chose to present their heat-transfer rate data based on Nusselt and Rayleigh numbers in which the relevant length dimension is taken as the vertical distance from the “origin” of the boundary layer, i.e., the bottom of the hot wall and the top of the cold wall. The temperature difference was taken as the magnitude of the difference between the wall and core temperature. On this basis the present computations for the two walls essentially form a single set of results, shown by the solid line in Figure 10. The sudden steepening of the curve for $Ra_y \approx 3 \times 10^7$ corresponds to a height where turbulent transport coefficients augment significantly. Now, the experimental data on the cold side of the cavity align rather pleasingly with the predictions, while those on the hot side lie about 30% higher than the computations, at least for Ra up to 2×10^9 . One contributor to this discrepancy seems to be that the heat loss through the side walls of the cavity induces a greater heat inflow through the hot wall than in the computations, giving a somewhat higher level of Nu .

The overall performance of the present procedure in computing cavity heat transfer can be assessed from Figure 11. The dependence of the mean Nusselt number \bar{Nu} has been investigated by Cowan *et al.*²² and by McGregor and Emery.²³ Their experimental study suggested, perhaps surprisingly, that there was no significant effect of aspect ratio, their data being well correlated by an equation of the form

$$Nu = c Ra^{1/3} \tag{10}$$

where, according to McGregor and Emery,²³ the constant c was 0.046 while Cowan *et al.*²² proposed the value of 0.043. In the above, Nu and Ra are based on cavity width and temperature difference between the vertical plates. Figure 11 shows computations obtained in the present study: several runs have been made for the infinitely tall cavity and one each with uniform wall temperatures for aspect ratios of 10:1, 5:1, and 1:1. These suggest that \bar{Nu} does indeed increase as $Ra^{1/3}$ and that the effects of aspect ratio are small. All our finite-cavity computations are well represented by Equation 10, the optimum choice of c being approximately 0.047. The same value of the coefficient also gives very close agreement with our computations for a 30:1 cavity. We recall that, in this case, to match the experiment the heated wall had a uniform heat flux applied to it. The correlation therefore needs to be converted to one based on Ra_q , the Rayleigh number based on wall heat flux rather than on temperature difference. Since $Ra_q \equiv \bar{Nu} Ra$, Equation 10 with $c = 0.047$ now becomes

$$\bar{Nu} = 0.1 \bar{Ra}_q^{1/4} \tag{11}$$

a form which agrees with our computed result within 2%. The infinite-cavity computations give levels of \bar{Nu} a little higher than the finite-cavity results, for $Ra > 3 \times 10^7$ the implied value of the coefficient c being 0.050.

The final topic considered is the appropriateness of the buoyant flow wall laws for velocity and temperature recommended in Ref. 1. Over a more than twofold variation of Rayleigh number, George and Capp showed that measured temperature profiles in natural convection boundary layers on a vertical plate were very well described by

$$\frac{\Delta\Theta}{\Delta\Theta_w} = 1 - 0.1 \left(\frac{x}{\eta_\theta} \right), \quad 0 \leq \frac{x}{\eta_\theta} \leq 1.7 \tag{12a}$$

$$= 1.45 \left(\frac{x}{\eta_\theta} \right)^{-1/3}, \quad 1.7 \leq \frac{x}{\eta_\theta} \tag{12b}$$

where $\eta_\theta \equiv [\lambda^2 g \Delta\Theta_w]^{1/3}$ and $\Delta\Theta$ is the local temperature above the surroundings. The corresponding profile recommended for the velocity was

$$V^* \equiv \frac{V}{(g \Delta\Theta_w \lambda / \theta)^{1/3}} = 12.3 \left(\frac{x}{\eta_\theta} \right)^{1/3} - 9.3, \quad 1.7 \leq \frac{x}{\eta_\theta} \tag{13}$$

Here λ denotes the thermal diffusivity $\kappa/\rho c_p$ and the values of the coefficients in Equations 12 and 13 are those appropriate to a Prandtl number of about 0.7.

For the one-dimensional infinite buoyant cavity test reported earlier, a number of solutions were obtained for different distances between the vertical walls or, effectively, for different Rayleigh numbers. The results are plotted in Figure 12 using the normalized velocity, temperature, and distance scales of

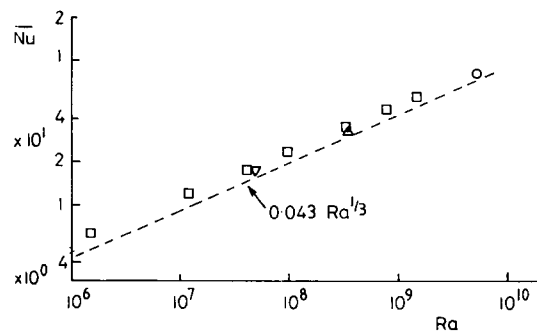


Figure 11 Mean Nusselt number in closed cavities: computations: \circ 1:1; \triangle 5:1; ∇ 10:1; \square ∞

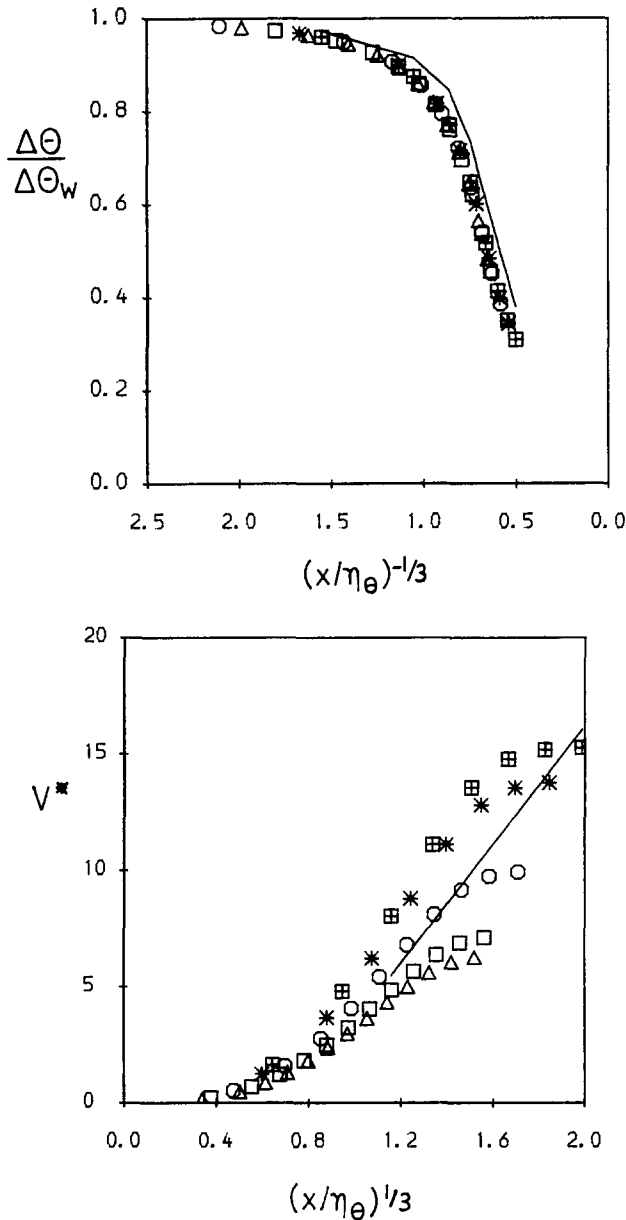


Figure 12 Near-wall profiles in George and Capp coordinates: (a) temperature; (b) vertical velocity; \boxplus $Ra=3.5 \times 10^8$; $*$ $Ra=1.2 \times 10^8$; \circ $Ra=1.5 \times 10^7$; \square $Ra=2.9 \times 10^8$; \triangle $Ra=8.2 \times 10^8$; — George and Capp "universal" profiles

Equations 12 and 13, with $\Delta\Theta$ now indicating the temperature excess over that at the midplane. It is clear that our numerical solutions of the temperature do indeed collapse onto a single curve consistent with the proposed thermal relations but that the velocity profiles do not: in the chosen coordinates, for each Rayleigh number, a quite distinct velocity distribution is traced. A possible reason for this failure to align with the near-wall profile reported for turbulent natural convection on a vertical plate is that in the present flow the outer regions are far more energetic and are thus more likely to affect the near-wall structure. A second, and probably more important, factor is that the Rayleigh numbers of this study are not high enough for viscous stresses to be negligible in the near-wall region. For example, at the position of maximum velocity the turbulent viscosity is less than five times the molecular value, even at the highest value of Rayleigh number. It is true that for $\overline{Ra} > 10^8$

the near-wall velocity profile does seem to be approaching an asymptotic form in George-Capp coordinates, but that asymptote lies well above Equation 13. In fact, To and Humphrey's² ASM computations of natural convection on a vertical flat plate accord closely with the present results as far as the near-wall velocity and temperature profiles are concerned. These workers also showed that their computations agreed closely with the experiments of Miyamoto *et al.*²⁴ and Cheesewright and Ierokipiotis.²⁵ Indeed, the present computations, like those of Ref. 2 and the cited experiments, all support an asymptotic velocity law of the form

$$V^* = 16.5(x/\eta_\theta)^{1/3} - 11.3 \quad (14)$$

proposed by To and Humphrey.²

Conclusions

The following principal conclusions have emerged from this computational study of buoyantly driven flow in closed cavities:

- In confirmation of finite-element results of Betts and Dafa'Alla,⁶ the usual forms of the low-Reynolds-number $k-\epsilon$ turbulence model (e.g., Refs. 12 and 13) do not succeed in predicting the correct flow rate and heat transfer for the infinite cavity.
- However, by introducing an additional source term to the energy dissipation (ϵ) equation, as proposed recently by Yap¹⁸ from his study of forced convection in separated flows, agreement with experiment is achieved within the uncertainty associated with lack of two-dimensionality of the data and ignorance about precise thermal boundary conditions. The validity of this modification is demonstrated for both the 30:1 and the 5:1 cavities, though its effect is only important in the former case.
- The predictions of flow in an infinite cavity strongly support the proposals of George and Capp¹ for the near-wall temperature profile. The corresponding proposal for the near-wall velocity profile is, however, not in accord with the present computations, partly because of the relatively low Rayleigh numbers here considered. While our work is not in conflict with the idea of a universal velocity profile at high Rayleigh numbers, our results tend to support the modified formula of To and Humphrey.

Acknowledgments

We are pleased to acknowledge helpful discussions with Dr. R. Cheesewright on the data obtained by his group and numerous constructive comments by the referees. Mrs. L. J. Ball has prepared the manuscript with appreciated care.

Some of the results reported here have been presented at the 2nd UK National Heat Transfer Conference, Strathclyde, 14-16 September 1988.

References

- 1 George, W. K. and Capp, S. P. *Int. J. Heat Mass Transfer*, 1979, **22**, 813
- 2 Humphrey, J. A. C. and To, W. M. *Int. J. Heat Mass Transfer*, 1985, **29**, 573
- 3 Cotton, M. and Jackson, J. D. Calculation of turbulent mixed convection in a vertical tube using a low-Reynolds number $k-\epsilon$ turbulence model. Paper 9-6, *Proc. 6th Turbulent Shear Flows Symp.*, Toulouse, 1987
- 4 Cotton, M. PhD Thesis, Faculty of Science, University of Manchester, 1987

- 5 Betts, P. L., Dafa'Alla, A. A., and Haroutunian, V. Low Reynolds number modelling of the wall region for turbulent natural convection in a tall cavity. *Proc. 4th Int. Conf. on Numerical Methods in Laminar and Turbulent Flow*, Pineridge Press, Swansea, 1985
- 6 Betta, P. L. and Dafa'Alla, A. A. Turbulent buoyant air flow in a tall rectangular cavity. *Significant questions in buoyancy-affected enclosure or cavity flows*, HTD-60, ASME Winter Annual Meeting, Anaheim, December 1986, p. 83
- 7 Plumb, D. A. and Kennedy, C. A. *ASME J. Heat Transfer*, 1977, **99**, 79
- 8 Patel, V. C., Rodi, W., and Scheuerer, G. *AIAA J.*, 1985, **23**, 1320
- 9 Ince, N. Z. Experimental and numerical study of natural convection in tall cavities, PhD Thesis, Faculty of Technology, University of Manchester, 1984
- 10 Dafa'Alla, A. A. Turbulent natural convection in a tall closed cavity, PhD Thesis, Faculty of Technology, University of Manchester, 1988
- 11 Cheesewright, R., King, K. J., and Ziai, S. Experimental data for the validation of computer codes for the prediction of two-dimensional buoyant cavity flows. *Significant questions in buoyancy affected enclosure or cavity flows*, HTD-60, ASME Winter Annual Meeting, Anaheim, December 1986, p. 75
- 12 Jones, W. P. and Launder, B. E. *Int. J. Heat Mass Transfer*, 1972, **15**, 301
- 13 Launder, B. E. and Sharma, B. I. *Letters in Heat Mass Transfer*, 1974, **1**, 131
- 14 Lin, C. J. and Churchill, S. W. *Num. Heat Transfer*, 1978, **1**, 129
- 15 Daly, B. J. and Harlow, F. H. *Phys. Fluids*, 1970, **13**, 2634
- 16 Hanjalic, K. and Launder, B. E. *J. Fluid Mech.*, 1972, **52**, 609
- 17 Rodi, W. and Scheuerer, G. Scrutinizing the $k-\epsilon$ model under adverse pressure-gradient conditions. *Proc. 4th Turbulent Shear Flows Symp.*, Karlsruhe, 1983, 2-8
- 18 Yap, C. Turbulent heat and momentum transfer in recirculating and impinging flows, PhD Thesis, Faculty of Technology, University of Manchester, 1987
- 19 *Proc. 3rd Biennial Colloquium on Computational Fluid Dynamics*, UMIST, Manchester 1988
- 20 Huang, P. G. and Leschziner, M. A. An introduction and guide to the computer code TEAM. UMIST Mechanical Engineering Dept. Rep., July 1983
- 21 Cheesewright, R. and Ziai, S. Distributions of temperature and local heat transfer rate in turbulent natural convection in a large cavity. Paper NS-03. *Proc. 8th Int. Heat Transfer Conf.*, San Francisco, August 1986
- 22 Cowan, G. H., Lovegrove, P. C., and Quarini, G. L. Turbulent natural convection heat transfer in vertical, single, water-filled cavities. Paper 2NC13, *Proc. 7th Int. Heat Trans. Conf.*, 1982, 195
- 23 McGregor, R. K. and Emery, A. F. *ASME J. Heat Transfer*, 1969, **91**, 391
- 24 Miyamoto, M., Kajino, H., Kurima, J., and Takanami, I. Development of turbulence characteristics in a vertical, free convection boundary layer. *Proc. 7th Int. Heat Transfer Conf.*, 1982, **2**, 323-328
- 25 Cheesewright, R. and Ierokipiotis, E. *Proc. 7th Int. Heat Transfer Conference*, 1982, **2**, 305-391